

Force-Driven Traffic Simulation for a Future Connected Autonomous Vehicle-Enabled Smart Transportation System

Yuming Zhang, Guohui Zhang¹, Rafael Fierro, and Yin Yang

Abstract—Recent technology advances significantly push forward the development and the deployment of the concept of *smart*, such as smart community and smart city. Smart transportation is one of the core components in modern urbanization processes. Under this context, the connected autonomous vehicle (CAV) system presents a promising solution towards the enhanced traffic safety and mobility through state-of-the-art wireless communications and autonomous driving techniques. Being capable of collecting and transmitting real-time vehicle-specific, location-specific, and area-wide traffic information, it is believed that CAV-enabled transportation systems will revolutionize the existing understanding of network-wide traffic operations and reestablish traffic flow theory. This paper develops a new continuum dynamics model for the future CAV-enabled traffic system, realized by encapsulating mutually-coupled vehicle interactions using virtual internal and external forces. Leveraging Newton's second law of motion, our model naturally preserves the traffic volume and automatically handles both the longitudinal and lateral traffic operations due to its 2-D nature, which sets us apart from the existing macroscopic traffic flow models. Our model can also be rolled back to handle the conventional traffic of human drivers, and the experiment shows that the model describes real-world traffic behavior well. Therefore, we consider the proposed model a complement and generalization of the existing traffic theory. We also develop a smoothed particle hydrodynamics-based numerical simulation and an interactive traffic visualization framework. By posing user-specified external constraints, our system allows users to visually understand the impact of different traffic operations interactively.

Index Terms—Smart transportation, connected vehicle, autonomous vehicle, traffic flow model, visualization, SPH, particle system, numerical solution.

I. INTRODUCTION

THE concept of smart transportation has drawn more and more attention while addressing important challenges and concerns like traffic congestion, fuel consumption, air pollution and so on. Emerging Connected

Vehicle (CV) and Autonomous Vehicle (AV) technologies can improve network-wide traffic safety, mobility, and operation efficiency through real-time Dedicated Short Range Communications (DSRC) based Vehicle-to-Vehicle (V2V) and Vehicle-to-Infrastructure (V2I) communications [1]–[3]. The research team at the University of Toronto including Alberto Leon-Garcia, Hans-Arno Jacobsen, Baher Abdulhai, etc. conducted pioneering work to establish the Connected Vehicles and Smart Transportation (CVST) portal to share live integrated traffic information in CV environments [4]–[7]. Many other researchers in the university investigated driving challenges and opportunities in AV-enabled traffic systems [8], [9]. According to the Research and Innovative Technology Administration (RITA) of the U.S. Department of Transportation (USDOT), 81% of all vehicle-involved crashes can be avoided or significantly mitigated based on CV techniques annually. Meanwhile, AV is capable of sensing its environment and self-piloting based on navigation hardware such as cameras, radar, Lidar, laser rangefinders, and GPS. AVs can much more accurately judge distances and velocities, attentively monitor their surroundings, and react instantly to emergent situations. By combining CV and AV technologies seamlessly, it is believed that Connected Autonomous Vehicle or CAV enabled traffic systems can revolutionize the existing understanding of vehicle-infrastructure interactions and network-wide traffic system operations. However, the existing traffic theory becomes awkward when comes to the context of CAV. Existing traffic flow models [10]–[18] were developed for Human Driven Vehicle (HDV)-based traffic flow operations based on one-way coupled vehicle interactions adopted in classic car-following models (a following vehicle adjusts its operation conditions, such as acceleration/deceleration only based on its leading vehicle's position, relative speed difference, etc.). To incorporate the lateral traffic flow operations, additional lane-changing models must be involved. Enabled by CAVs, the two-way communication and collaborative linkages among CAVs can greatly facilitate us to formulate the mutually-coupled vehicle interactions (not only a following vehicle will be impacted by its leading vehicle, but also the leading vehicle will be impacted by its following vehicle and its surrounding vehicles too) for CAV-enabled traffic flow. This feature implies that CAVs are expected to move freely along both the longitudinal and lateral direction and a two-dimensional traffic flow model could be more reasonable. Currently, an aggregated macroscopic

Manuscript received April 27, 2017; revised September 6, 2017 and November 21, 2017; accepted December 2, 2017. Date of publication April 17, 2018; date of current version June 28, 2018. The work of Y. Zhang and Y. Yang was supported in part by the NSF under Grant CHS-1464306, Grant CHS-1717972, and Grant CNS-1637092, and in part by nVidia GPU grant. The Associate Editor for this paper was S. Djahel. (*Corresponding author: Guohui Zhang.*)

Y. Zhang, R. Fierro, and Y. Yang are with the University of New Mexico, Albuquerque, NM 87131 USA (e-mail: yumingzhang@unm.edu; rfierro@unm.edu; yangy@unm.edu).

G. Zhang is with University of Hawaii at Manoa, Honolulu, HI 96822 USA (e-mail: guohui@hawaii.edu).

Color versions of one or more of the figures in this paper are available online at <http://ieeexplore.ieee.org>.

Digital Object Identifier 10.1109/TITS.2017.2787141

1524-9050 © 2018 IEEE. Personal use is permitted, but republication/redistribution requires IEEE permission.
See http://www.ieee.org/publications_standards/publications/rights/index.html for more information.

model for CAV-based traffic is still an under-investigated problem.

Motivated by this fact, we present a new traffic flow model for mutually-coupled vehicles enabled by CAV techniques. Under this scenario, an individual vehicle spontaneously seeks for its local optimal configurations¹ based on the real-time information shared/obtained from the surroundings. Such behavior exaggerates intrinsic physics traits of the system, making the CAV-enabled traffic resemble other real-world continuum systems like fluid or molecular systems. We use several virtual internal and external forces to describe the two-way vehicle-vehicle interaction. By leveraging Newton's second law of motion, our model naturally preserves the traffic volume, which is required as a macroscopic traffic flow model, and automatically handles both the longitudinal and lateral traffic operations. While our model is designed for CAV-enabled traffic, it can be easily rolled back to simulate the regular traffic of human drivers. The experiment shows that the proposed model describes the real-world traffic behavior well. Therefore, we consider the proposed model a generalization of the existing traffic theory. We also develop a Smoothed Particle Hydrodynamics or SPH based numerical simulation and an interactive traffic visualization framework.

The rest of this paper is organized as follows: a brief literature review is given in Section II. Section III explains our force-driven model and how it can be numerically simulated using SPH. The system implementation details are provided in Section IV, followed by the discussion of experimental results in Section V. This research effort is concluded with future work in Section VI.

II. RELATED WORK

CAV technology has been developed and demonstrated great potential to transform the way people travel through the interconnected network including cars, buses, trucks, trains, traffic signals, cell phones, and other devices [19]. Litman concluded that AVs will consist of about 50% of vehicle fleet, 90% of vehicle sales, and 65% of all vehicles by 2050 [20], although the true anticipated market share needs more solid verifications and investigations as a research question. As an echo to such rapid deployment of CAV, many research efforts have been devoted to explore how CAV technology can improve the existing transportation system. Ni *et al.* [21] proposed a car-following model incorporating the effects of CV technology and investigated the highway capacity gain. Acceleration-based connected cruise control was proposed to increase roadway traffic mobility through wireless V2V communication [22], [23]. An algorithm using CV data was proposed to minimize the vehicle delay and queue length at intersections [24]. Multiple studies have been conducted on applications of CV technology, including traffic monitoring [25], ramp metering [26], route guidance [27], [28], traffic signal control [29]–[32], vehicle-infrastructure-integration

implementation issues [33], and public transportation [34]. While most applications of CV technologies were assumed to be effective based on perfect V2V and V2I communications, it was pointed out that wireless communications could also experience packet delays/drops, which might lead to a serious downgrade of CV applications [35], [36]. In CAV-enabled traffic systems, vehicle interactions are dramatically changed from one-way to all-directional neighborhood-wide information dissemination, which calls for a new macroscopic traffic flow formulation [37].

Traditional continuum traffic flow models were pioneered by Lighthill and Whitham [10] and Richards [11] to mathematically describe macroscopic traffic flow operations (known as the LWR model) based on a nonlinear conservation law. Many researchers introduced other high-order traffic flow models [12]–[14]. In recent work, Cheng *et al.* [38] proposed a new continuum traffic flow model incorporating the effects of drivers' timid and aggressive behavior. Andreianov *et al.* [17] employed point constraints in a second-order traffic flow model for modeling some traffic conditions, for instance, traffic signals. Wang *et al.* [18] used the energy conservation law to develop a two-regime speed-density formulation for the first-order traffic flow model. Zheng *et al.* [39] proposed a flexible traffic stream model connecting four driving behavior-related parameters to the fundamental diagram (i.e. the fundamental relationships among the flow, speed and density). All those macroscopic models are one-dimensional and focus on conventional traffic.

On the other hand, microscopic traffic flow models, or agent-based models, describe the car-following behavior and the lane-changing behavior of individual vehicles. There have been different microscopic models due to their specific assumptions of the flow behavior [40]. The acceleration of the following vehicle is a function of a calibration constant, a reaction time, its velocity, and the velocity of the preceding vehicle relative to it. Recently, Asaithambi *et al.* [41] provided a review of current microscopic driving behavior models and discussed both the longitudinal and lateral movements in mixed traffic. Guo *et al.* [42] proposed an improved car-following model that incorporates the effects of multiple preceding vehicles' velocity fluctuation feedback. Li *et al.* [43] introduced a sensitivity factor to the classic car-following model so that the vehicles in traffic are divided into two types as low- and high-sensitivity vehicles and used the linear stability theory to analyze the stability of the new model. To find out the relationship between the microscopic and macroscopic traffic flow model, Garavello and Piccoli [44] coupled the car-following model to the LWR model through suitable boundary conditions, for example, at the location $x = 0$. Holden and Risebro [45] proved that the car-following model converges to the LWR model when traffic becomes dense. To calibrate the model parameters, Chiappone *et al.* [46] used a genetic algorithm based on specific fundamental diagrams. In their method, the calibration is formulated as an optimization problem whose objective is to minimize the difference between the simulated and real data. Given the trajectory data collected from CVs, Zhu and Ukkusuri [47] proposed an optimal estimation approach for

¹Generally speaking, local optimal configurations mean the best position and velocity that a CAV can have in order to, for example, reach the highest possible traveling speed or have the shortest traveling time. The objective is to improve the traffic mobility and maximize the transportation capacity.

calibrating the car-following behavior in a CVs and regular vehicles mixed traffic environment. Zhong *et al.* [48] adopted two approaches, the Cross-Entropy Method (CEM) and the Probabilistic Sensitivity Analysis (PSA) algorithm, for the calibration. The former is able to find the optimal set of the parameters, while the latter is applied to identify the most important parameters in order to reduce the computational burden. To predict the traffic flow, Zhao and Sun [49] developed a fourth-order Gaussian process dynamical model (GPDM) which is a unsupervised learning method suitable for modeling dynamic real-world traffic data. Their experiments showed that the proposed method outperformed the existing methods for traffic flow predictions.

The existing traffic simulation packages VISSIM, AIMSUN, Paramics, etc. are discrete event-driven, agent-based simulation applications to mimic how the traffic system operates today. Many other outstanding simulation model applications include [50]–[55]. Our developed new model is completely different from these simulation tools. To the best of our knowledge, no existing studies have been conducted to systemically investigate the CAV traffic flow model and simulate mutually-coupled vehicle interactions. Inspired by dynamic motion patterns of real-world natural continuum systems such as the elastic solid (e.g. a piece of deformable rubber), the viscous volume (such as honey drops or oily ointments) and the fluid (like water or smoke), we formulate the mutually-coupled vehicle interactions using virtual forces. Being free of the individual randomness in agent-based methods [56] and/or the limitation of one-way-coupled vehicle manipulation adopted in classic car-following models, we believe the proposed model is able to more accurately describe macroscopic traffic flow dynamics in the context of CAV-enabled traffic systems.

III. METHODOLOGY

In this section, we first explain how to formulate mutually-coupled vehicle interactions by the virtual forces. Based on it, the equation of motion of an elementary particle on the traffic can be formulated as the force equilibrium. This equation is aggregated to model the macroscopic traffic behavior. To do so, we have to resort to numerical computations, and we choose to use SPH in our paper. After the density and velocity at each particle is computed, the complete information of the CAV-enabled traffic is obtained.

A. Virtual Forces Driven Traffic Flow Model

We consider the CAV-enabled traffic as a 2D homogeneous dynamic continuum system, wherein all CAVs have identical operational characteristics. Sharing a similar spirit of other continuum traffic models' development [15], [16], our model is based on an analytical formulation of several external and internal *virtual forces* that allow mutually-coupled vehicle-vehicle and vehicle-environment interactions. In the remaining part of the paper, we use a bold lower-case letter like \mathbf{v} or \mathbf{u} to denote a vector-value quantity, and a regular letter like v or u to denote a scalar quantity.

1) *Virtual External Forces*: We explicitly define an external force that drives the traffic motion. Analogous to the gravity force, this force induces a constant acceleration field \mathbf{g} over the entire traffic heading to the destination. Should the roadway be curved, the acceleration always aligns with the roadway's tangent. As to be detailed in Section IV-B, we use the Bézier spline (with parameter p) to describe the roadway geometry, and the tangent vector can be calculated as $[\partial x/\partial p, \partial y/\partial p]^\top \in \mathbb{R}^2$. Clearly, the traffic speed driven by \mathbf{g} would approach an infinity if the roadway is sufficiently long. While such behavior maximizes the transportation capacity, it is always favored that the traffic velocity be capped by a certain limit. Therefore, we plug in another *damping force* \mathbf{f}_d that penalizes an excessively high-speed traffic. We use the *proportional damping* model [57] so that \mathbf{f}_d is linearly proportional to the traffic speed, yet along the opposite direction: $\mathbf{f}_d = -c\mathbf{u}$, where c is the *damping factor*. For a given speed limit \bar{u} , c can be computed as $\|\mathbf{g}\|/\|\bar{\mathbf{u}}\|$ so that \mathbf{f}_d completely cancels out \mathbf{g} when the speed limit is reached, and no further acceleration will be obtained. Putting together, the virtual external force at an arbitrary location on the traffic with density ρ is defined as:

$$\mathbf{f}_{ext} = \rho (\mathbf{g} - c\mathbf{u}). \quad (1)$$

2) *Virtual Internal Forces*: The virtual internal forces are devised to model the between-vehicle interaction in a CAV-enabled traffic based on the assumption that a CAV is aware of the traffic condition over a wider surrounding neighborhood.

Intuitively, vehicles tend to move from a high density area to a low density area,² and a *pressure force* \mathbf{f}_p is the resultant of such non-uniform density distribution following the negative direction of the density gradient. To incorporate various fundamental diagrams, we formulate this force as:

$$\mathbf{f}_p = -\nabla(k\rho^\gamma), \quad (2)$$

where k and γ are two positive constants related to a desired fundamental diagram.

Similar to \mathbf{f}_p , the *viscosity force* \mathbf{f}_v intends to make the velocity distribution uniform, i.e. a vehicle will accelerate when its neighbors are moving faster, or decelerate when its neighbors have lower velocity. Since velocity is essentially a vector field, we model \mathbf{f}_v using the *Laplacian* defined as the divergence of the velocity gradient:

$$\mathbf{f}_v = \nabla^2(\mu\mathbf{u}), \quad (3)$$

where μ is a constant coefficient. We note that \mathbf{f}_p and \mathbf{f}_v are two-dimensional vectors. Their components perpendicular to the current traffic direction allow the lane-changing behavior. If lane A has a lower vehicle density than lane B, vehicles on lane B are likely to switch to lane A due to the existence of \mathbf{f}_p . Likewise, if lane A is a high-speed lane, it is also more attractive to the traffic due to \mathbf{f}_v .

Lastly, the equation of motion of an elementary volume in the traffic can be written as the equilibrium of all the external

²Here the density is a *local* concept. For example, a vehicle tends to move from a congested lane to the adjacent lane with less traveling vehicles. One should not confuse it with the global traffic distribution in the entire city.

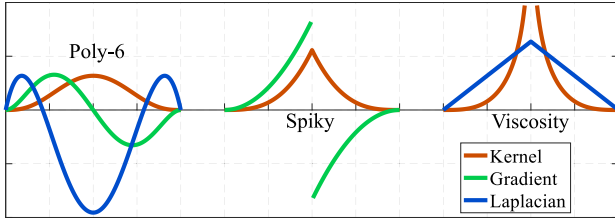


Fig. 1. We use the 2D poly-6, spiky and viscosity kernel for the SPH simulation. The spiky kernel is for the gradient evaluation needed for \mathbf{f}_p . The viscosity kernel is for the Laplacian evaluation of \mathbf{f}_v .

and internal virtual forces:

$$\rho \frac{\partial \mathbf{u}}{\partial t} = \rho (\mathbf{g} - c\mathbf{u}) - \nabla(k\rho^\gamma) + \nabla^2(\mu\mathbf{u}). \quad (4)$$

Equation (4) is essentially a reiteration of Newton's second law of motion. The left hand side of the equation is the inertial force (i.e. the mass times the acceleration) which should be balanced by all of the other forces being exerted.

3) *Discussion*: It can be seen that Equation (4) has a similar form of the *Navier-Stokes equation* [58]:

$$\frac{\partial \mathbf{u}}{\partial t} + \underbrace{(\mathbf{u} \cdot \nabla) \mathbf{u}}_{\text{Convection}} - \underbrace{\nu \nabla^2 \mathbf{u}}_{\text{Fluid viscosity}} = \underbrace{-\nabla \omega}_{\text{Thermodynamics}} + \mathbf{g}. \quad (5)$$

\mathbf{f}_v in Equation (3) is our counterpart of the fluid viscosity and $\mathbf{f}_p = -\nabla(k\rho^\gamma)$ is analogous to $-\nabla\omega$, the thermodynamic force. To satisfy the traffic volume conservation law, we employ the equivalent mass conservation constraint:

$$\frac{\partial \rho}{\partial t} + \nabla \cdot (\rho\mathbf{u}) = 0. \quad (6)$$

This constraint can be automatically satisfied in a Lagrangian method such as SPH (which is discussed in the following section), because all the differential volumes in the traffic are always tracked and computed.

B. Discretization and SPH

We discretize the continuous traffic flow with a particle system similar to the fluid simulation in [59]. One should note that a particle represents a small volume of the traffic flow and is not necessarily equivalent to a real vehicle. A particle carries many useful quantities such as the positional coordinates, the density, the acceleration, the velocity, and the id of the road where it is traveling. The state of the aggregated particles determines the entire traffic flow, i.e. the distribution of the density and velocity field.

SPH was invented to simulate astrophysical phenomena by Lucy [60] and Gingold and Monaghan [61] in 1977. It is essentially an interpolation method for a particle system [62], [63]. Unlike other numerical methods, for instance the well known finite difference method (FDM), SPH does not need a grid to evaluate the spatial derivatives. Instead, SPH uses the differentiation of the interpolation formula directly. This simplifies the computation. Although SPH is less accurate than FDM, it is general enough and has been adapted into the Computer Graphics community [59], [64], [65] for simulating various physical phenomena, such as water, lava and deformable soft

bodies. To have more details, we refer the interested readers to a wide-ranging list of the SPH papers (e.g. [59]–[65]).

The key idea in SPH is to use a non-negative smoothing kernel function W such that $\int W(\bar{\mathbf{r}} - \mathbf{r}, h) d\bar{\mathbf{r}} = 1$ to approximate the Delta function δ : $\lim_{h \rightarrow 0} W(\bar{\mathbf{r}} - \mathbf{r}, h) = \delta(\bar{\mathbf{r}} - \mathbf{r})$. Thus an integrable smooth function $A(\mathbf{r})$ can be written as:

$$A(\mathbf{r}) = \int A(\bar{\mathbf{r}}) \delta(\bar{\mathbf{r}} - \mathbf{r}) d\bar{\mathbf{r}} \approx \int A(\bar{\mathbf{r}}) W(\bar{\mathbf{r}} - \mathbf{r}, h) d\bar{\mathbf{r}}, \quad (7)$$

where $h > 0$ is the support radius. When the continuous function domain is discretized using a particle system, the integral in Equation (7) is also discretized as a summation:

$$A(\mathbf{r}) \approx \sum_{j \in \mathcal{N}} A_j \frac{m_j}{\rho_j} W(\mathbf{r}_j - \mathbf{r}, h), \quad (8)$$

where \mathcal{N} is the set of indices of the neighboring particles. Derivatives of $A(\mathbf{r})$ can be approximated in a similar way:

$$\nabla A(\mathbf{r}) \approx \sum_{j \in \mathcal{N}} A_j \frac{m_j}{\rho_j} \nabla W(\mathbf{r}_j - \mathbf{r}, h). \quad (9)$$

C. Numerical Simulation and Smoothing Kernels

The Gaussian kernel is a widely-used choice for smoothing kernel function W . However, the Gaussian kernel does not have a compact support (i.e. the support radius of the Gaussian is infinite), and it is expensive to evaluate. We follow the suggestions in [59], and employ three 2D polynomial smoothing kernels namely the *poly-6 kernel*, the *spiky kernel*, and the *viscosity kernel* to numerically compute necessary physical and kinematic quantities as shown in Fig. 1:

$$\begin{cases} W_{poly6}(\mathbf{r}, h) = \frac{4}{\pi h^8} (h^2 - \|\mathbf{r}\|^2)^3 \\ W_{spiky}(\mathbf{r}, h) = \frac{10}{\pi h^5} (h - \|\mathbf{r}\|)^3 \\ W_{viscosity}(\mathbf{r}, h) = \frac{40}{\pi h^2} \left[-\frac{\|\mathbf{r}\|^3}{9h^3} + \frac{\|\mathbf{r}\|^2}{4h^2} \right. \\ \left. - \frac{1}{6} \ln\left(\frac{\|\mathbf{r}\|}{h}\right) - \frac{5}{36} \right] \end{cases}$$

The poly-6 kernel possesses a Gaussian-like bell curve with a compact support, and it is easy to evaluate. It serves as the default kernel in our model. To evaluate \mathbf{f}_p however, the poly-6 kernel is not suitable because its gradient gets to zero as $\|\mathbf{r}\| \rightarrow 0$ (i.e. see Fig. 1). This property implies that when particles approach each other, \mathbf{f}_p becomes smaller and the particles tend to get clustered. This is not desired in a traffic flow. As a result, the spiky kernel with a high gradient value as $\|\mathbf{r}\| \rightarrow 0$ is used for computing \mathbf{f}_p . For a similar reason, we use the viscosity kernel for \mathbf{f}_v . The Laplacian of the viscosity kernel has a cone shape with its maximum at $\|\mathbf{r}\| = 0$, and it is positive within the support area which is required for the computation. All of these three kernels have vanished values when $\|\mathbf{r}\| > h$. Our experiments show that the three kernels work well in our traffic simulation. The gradient and Laplacian operators as appeared in Equations (2) and (3) for the spiky

and viscosity kernels can be evaluated as:

$$\begin{cases} \nabla W_{spiky}(\mathbf{r}, h) = -\frac{30}{\pi h^5} (h - \|\mathbf{r}\|)^2 \frac{\mathbf{r}}{\|\mathbf{r}\|} \\ \nabla^2 W_{viscosity}(\mathbf{r}, h) = \frac{40}{\pi h^5} (h - \|\mathbf{r}\|). \end{cases} \quad (10)$$

Note that SPH is a Lagrangian-style method, the convection term in Equation (5) is implicitly incorporated in our model. The unknown density ρ , as well as the associated virtual forces \mathbf{f}_p and \mathbf{f}_v (assuming \mathbf{g} is known) are calculated as:

$$\begin{aligned} \rho_i &= \sum_{j \in \mathcal{N}} m_j W_{poly6}(\mathbf{r}_j - \mathbf{r}_i, h) \\ \mathbf{f}_{p_i} &= -k \sum_{j \in \mathcal{N}} \frac{\rho_j^\gamma + \rho_i^\gamma}{2} \frac{m_j}{\rho_j} \nabla W_{spiky}(\mathbf{r}_j - \mathbf{r}_i, h) \\ \mathbf{f}_{v_i} &= \mu \sum_{j \in \mathcal{N}} (\mathbf{u}_j - \mathbf{u}_i) \frac{m_j}{\rho_j} \nabla^2 W_{viscosity}(\mathbf{r}_j - \mathbf{r}_i, h). \end{aligned}$$

Finally, the velocities and the new positions for the particles are computed using numerical time integration, and we are ready to simulate the traffic state of the next time instance.

D. Incorporating Existing Traffic Flow Models

So far, we have discussed a continuum model for CAV-enabled traffic, which uses two-dimensional internal and external forces for modeling the mutually-coupled CAV interactions. Most existing macroscopic traffic flow models based on conventional traffic are one-dimensional and incorporate various fundamental diagrams. A fundamental diagram is determined by the relationship between the density and velocity. For instance, the classic Greenshields model [66] presents a linear relationship between the density and velocity. In this subsection, we show that our model is versatile, and it can naturally be specialized to the conventional traffic. Therefore, the proposed traffic model could be considered a *generalization* of the existing traffic flow theory.

We downgrade our model to one-dimensional, and Equation (4) becomes:

$$\rho \frac{\partial u}{\partial t} = -k \frac{\partial (\rho^\gamma)}{\partial x} + \mu \frac{\partial^2 u}{\partial x^2} + \rho (g - cu). \quad (11)$$

If we consider a traffic equilibrium under a uniform velocity u_0 (f_v becomes zero in this case), without the external force, Equation (11) can be simplified as:

$$\rho \frac{\partial u}{\partial t} = -k\gamma \rho^{\gamma-1} \frac{\partial \rho}{\partial x}. \quad (12)$$

By the traffic volume conservation law (i.e. $\frac{\partial \rho}{\partial t} + u_0 \frac{\partial \rho}{\partial x} = 0$), we have:

$$\frac{\partial \rho}{\partial x} = -\frac{1}{u_0} \frac{\partial \rho}{\partial t}. \quad (13)$$

Combining Equations (12) and (13) yields:

$$\frac{\partial u}{\partial t} = k\gamma \rho^{\gamma-2} \frac{1}{u_0} \frac{\partial \rho}{\partial t}.$$

Integrating both sides of the above equation leads to:

$$u = \begin{cases} \frac{k}{u_0} \ln \rho + C & \gamma = 1 \\ \frac{k\gamma}{u_0(\gamma-1)} \rho^{\gamma-1} + C & \text{otherwise,} \end{cases}$$

where C is a constant. As mentioned previously, k and γ are parameters related to the desired traffic fundamental diagram. When we take $\gamma = 2$, we obtain the linear regression relation $u = \frac{2k}{u_0} \rho + C$, which is the classic Greenshields model [66]. Other fundamental diagrams, especially in polynomial relationships between the density and velocity, could be derived similarly by adjusting parameters k and γ .

The SPH-based simulation can also be easily degenerated to 1D, and the 1D poly-6 kernel is:

$$W_{poly6}(x, h) = \frac{35}{32h^7} (h^2 - x^2)^3.$$

Note that this formulation is slightly different from its 2D counterpart due to the unity requirement of the kernels.

In the conventional traffic, a vehicle only interacts with its leading vehicle. As a result, *we only use the positive half of the kernel function* when computing f_p and f_v . That is the summation is only over the particles in front of the current particle. The gradient and Laplacian of the 1D spiky and viscosity kernel are:

$$\begin{aligned} \frac{\partial W_{spiky}}{\partial x} &= -\frac{6}{h^4} (h-x)^2 \\ \frac{\partial^2 W_{viscosity}}{\partial x^2} &= \frac{12}{h^4} (h-x). \end{aligned}$$

IV. SYSTEM IMPLEMENTATION

Based on the derived traffic model and the SPH simulation, we develop an interactive visual traffic simulation system. Our system is implemented using Microsoft Visual C++ on a desktop Windows 10 PC with Intel Xeon E5-2670 CPU and 32G on-board memory. The traffic simulator was developed under Qt software development environment with the visualization based on OpenGL.

A. System Overview

Our CAV-enabled traffic simulation platform consists of three modules as outlined in Fig. 2. In the *input module*, the user specifies necessary traffic parameters (such as the expected traffic volume, traffic flow rates, and speed limits), roadway geometries and external constraints. External constraints are prescribed configurations of the traffic. For instance, users can force the velocity of the traffic at a given region to be zero to study the shockwave propagation, or they can block two out of four lanes of the roadway to test the resulting traffic congestion. The *simulation module* sets up the corresponding boundary conditions and kernel functions. We employ a full-kernel specification for CAV-enabled traffic simulation and a half-kernel specification for conventional traffic simulation. The core component of the simulation module is the SPH simulator. At each time step, the densities and velocities are calculated at all the particles. The continuous density and velocity field can then be interpolated. The

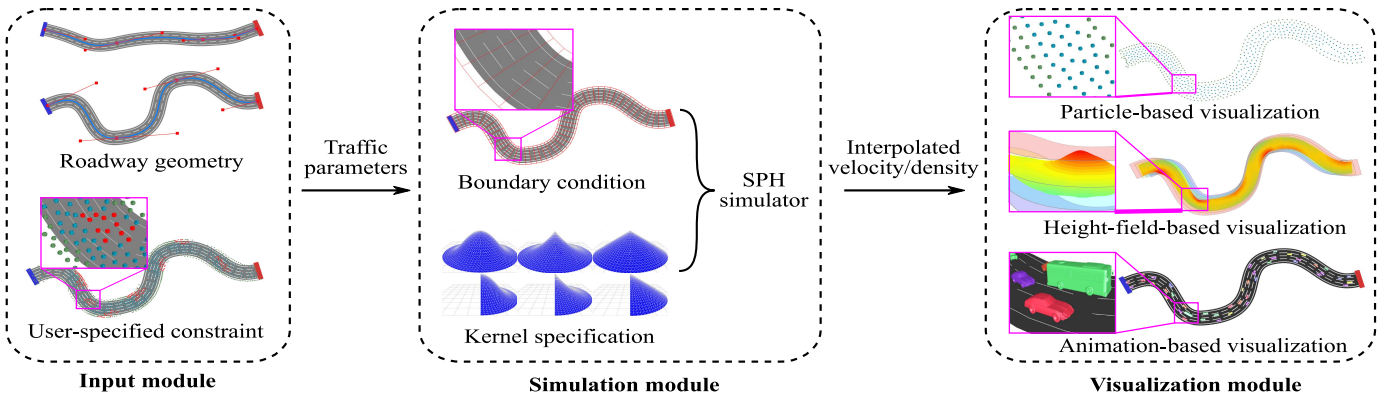


Fig. 2. A high-level flow chart of the proposed CAV-enabled traffic simulation framework. Our system has three major modules namely the input module, the simulation module, and the visualization module. The input module provides an interface for the user to fully specify the configurations of the traffic to be simulated. This information is passed to the simulation module, which will choose necessary boundary conditions and kernel functions (according to user's specification) and run a SPH-based simulation. The output will be leveraged in the visualization module to deliver the final visual representations of the simulated traffic flow.

visualization module uses the interpolated data obtained from the simulation module to animate and visualize the traffic flow.

Our system provides three levels of detail for the visualization. The user is able to view the simulated traffic as a discretized particle system. The density/velocity distribution can also be rendered as a height field in 3D with a customizable color map. The user can further zoom in the traffic to see animated vehicles. This detailed microscopic traffic visualization could be important and useful in applications like virtual reality or gaming. We create a database consisting of various 3D vehicle models (vans, sedans, trucks, etc.), then randomly pick the models and scatter them over the simulated traffic flow following the density distribution, so that more vehicles are rendered and animated at high-density regions. At the starting end of the road, the vehicles are generated according to the user-specified traffic flow rate (with the unit of vehicle per hour). The traffic flow rate is also converted to the boundary condition for generating particles for the SPH simulation (e.g. a vehicle is equivalent to ten particles). In this way, the traffic volume represented by the particles is consistent with the 3D vehicle models. Based on the position within the traffic at each animation frame, the i^{th} vehicle will have a velocity \mathbf{u}_i according to the SPH simulation, and its position \mathbf{x}_i for the next frame will be updated as $\mathbf{x}_i \leftarrow \mathbf{x}_i + \Delta t \mathbf{u}_i$. Here Δt denotes the time interval between two consecutive animation frames.

The graphical user interface (GUI) of our implemented system is shown in Fig. 3. It contains a main interface, four tabs, and other simulation controls. The first tab contains two sub-windows for the density/velocity field visualization. The second tab (Fig. 3 (b)) reports the density/velocity plots at positions of interest in the traffic, which can be interactively specified by the user. The third and fourth tabs provide miscellaneous functions/options for interactive settings, such as roadway geometries, constraints, kernels, forces, rendering options, and file I/O, as shown in Fig. 3 (c) and (d).

B. Roadway Geometries

To build up a realistic roadway segment, we use a cubic Bézier spline to model the roadway geometry variation at its

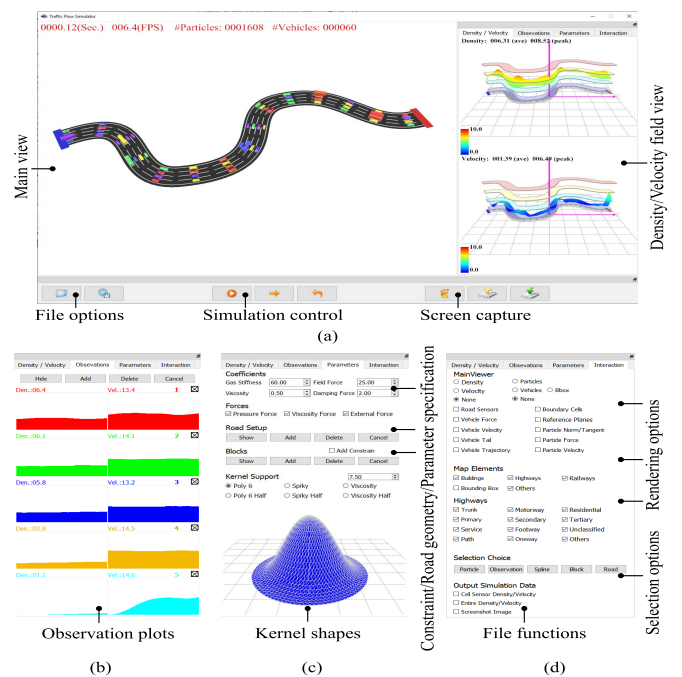


Fig. 3. The snapshot of the graphical user interface of the implemented system. Besides the major 3D visualization window, our system provides multiple mutually-linked plots, statistics and visualization sub-views. Most of them can be interactively controlled by the user to provide the desired visual perception of the traffic.

center line (known as the neutral axis too). The Bézier spline is a sequence of piece-wise cubic polynomial curves that are connected smoothly. We further extend the roadway segment to 2D by specifying the vertical span of the splines along the normal direction (i.e. the direction perpendicular to the tangent of the splines or the traffic direction). With this method, we can model various roadways with arbitrary shapes and widths (see the input module in Fig. 2). A roadway segment is further divided into a few polygons or *cells*. All cells together form the simulation domain of the roadway segment (see the simulation module in Fig. 2).

We set the cells to be wider than the roadway segment by two support radii, so that the particles along the roadway

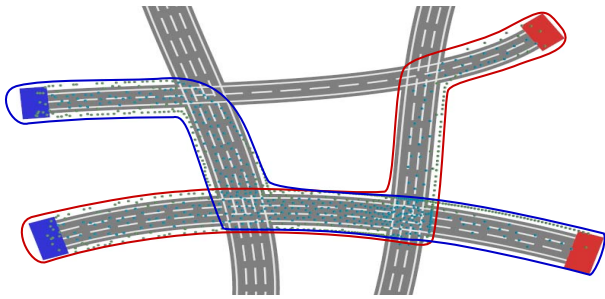


Fig. 4. Two traffic flow pieces are simulated in their associated simulation domains (highlighted in the blue and red frame). In the overlapping domain, the simulation result is the linear combination of these two pieces.

boundary can have a full support. This treatment smooths the boundary of the resulting density/velocity field. The particles outside of the roadway boundary serve similarly as the so-called ghost particles, which is a popular method in SPH simulation for boundary treatment [67]–[69]. We pre-compute and build a query table, whose entries are indices of the cells. The corresponding context includes many useful attributes associated with the cell, such as the road id, positional coordinates, tangent and normal vectors. The cells can also be used for fast boundary treatment. We employ the explicit project-and-reflect method: the particle is simply projected to the boundary where it is closest to once it moves out of the boundary [70]. With the cell-based subdivision, the roadway boundary becomes a piece-wise line segment, and it is trivial to project out-of-road particles back onto the boundary.

C. Simulation in Roadway Networks

A roadway network can be described as a collection of roadway segments connected by intersections. We divide the entire traffic flow in the roadway network into many small pieces. Each piece is in fact the aggregation of all vehicles with the similar trajectories. The user-specified trajectory data may come from real-world traffic or predicted traffic scenarios. The trajectories then determine the simulation domain associated with each piece which usually consists of a set of connected roadway segments. The simulation result is the linear combination of the simulation of all the pieces. Fig. 4 illustrates two traffic flow pieces and their associated simulation domains. In the overlapping domain, the simulation result is the linear combination of these two pieces.

In the conventional traffic, the intersection configurations are converted to the boundary conditions, for example, a red traffic signal phase imposes the zero-velocity constraint in the area. In the future CAV-enabled traffic, the traffic signals could be potentially removed. No additional constraints are applied to the intersection, and the traffic flow becomes uninterrupted in the entire roadway network. Our model works well in both of these two scenarios.

D. Fast Neighbor Search

The most expensive computation along the simulation is the summation over the neighborhood for all the particles (i.e. Equations (8) and (9)). Because particles are moving along

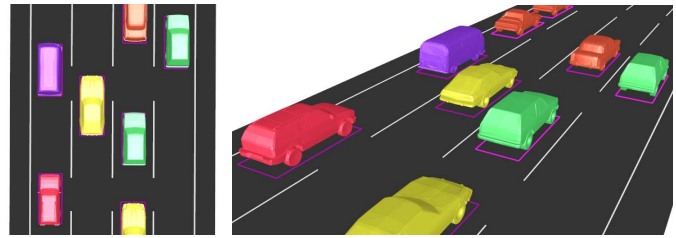


Fig. 5. The detailed traffic visualization uses animated 3D vehicle models to provide users an intuitive impression of the traffic. Each vehicle possesses a bounding box (the purple rectangle), which will be used for collision detection and handling.

the simulation, each particle's neighbors within the support radius also vary at each time step. A brutal force iteration overall the particles leads to a $\mathbf{O}(N^2)$ calculation which is expensive noting that it is only for a single animation frame. To accelerate this procedure, we employ the spatial hashing method [71] to fast retrieve the information of neighboring particles. Therefore, the time complexity of the simulation becomes linear with respect to the total number of particles.

E. Collision Detection and Handling

In the microscopic zoomed-in traffic visualization, we use animated 3D vehicle models to represent the traffic detail as shown in Fig. 5. Each rendered vehicle follows the position-dependant velocity obtained from the simulation. Because our force-based traffic model is an aggregated one, and it does not account for the microscopic vehicle behavior, it is possible that the animated vehicles collide each other. The collision detection is achieved by checking the overlapping region between 2D boundary boxes of the 3D vehicle models. Once a collision is detected, we roll back the simulation and apply a virtual *penalty force* to push the colliding vehicles away. It can be understood as connecting a vehicle with its neighbors by invisible springs, and the spring force will be triggered if a collision is detected and pulling the involved vehicles back.

V. EXPERIMENTAL RESULTS

Since CAV technique has not yet been widely deployed, we downgrade our model to the classic Greenshields model (i.e. as discussed in Section III-D), and then validate the model by calibrating the simulation result with the real-world traffic data. Afterwards, we simulate the CAV-enable traffic under various scenarios by imposing user-specified external constraints.

A. Model Validation

First, we show that our simulation based on the downgraded model well matches the real-world traffic observation. The ground-truth data are collected from the 11 inductance loop detector stations along State Route 520 in the greater Seattle areas in the State of Washington. These loop detector stations are selected because this roadway segment is one major corridor crossing the Lake of

TABLE I
SIMULATION PARAMETERS

Parameters	Values
γ	2.0
time step Δt	0.025s
support radius h	52ft
particle mass m	40.0
pressure coefficient k	6.0
viscosity coefficient μ	1.0×10^4
external acceleration g	60.0
damping factor c	2.0

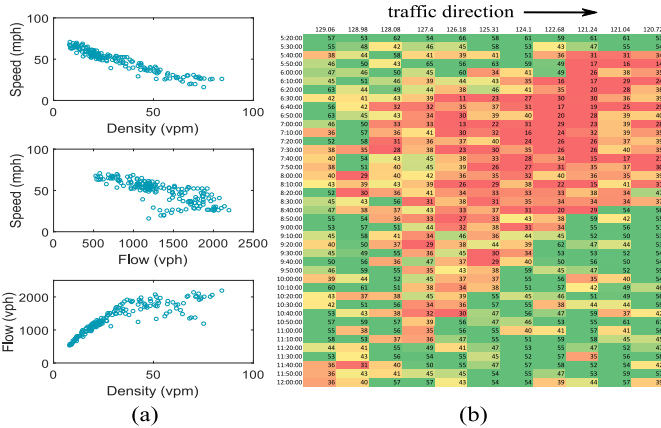


Fig. 6. The real-world traffic data are collected on State Route 520 in Seattle, Washington. The correlation between the flow, speed and density is given in (a), and the speed distribution is shown in (b) wherein the congestion is occurred and dissipated. The time interval between two rows is 10 minutes. Each column corresponds to a speed sensor. The red color indicates a low speed, while the green color indicates a relative high speed.

Washington, and the uninterrupted traffic flow is well characterized to minimize the on-ramp and off-ramp traffic disruption. Both stationary and dynamic characteristics of the traffic flow are considered. Fig. 6 (a) shows the general correlation among the traffic flow, speed, and density when the traffic becomes stationary (i.e. the fundamental diagram). Fig. 6 (b) plots the dynamic shockwave transmission and dissipation of the congestion during the morning peak-hour time period form 5:40 to 8:30 AM. The horizontal axis is the loop station milestone and the vertical axis gives the time instant stamp.

We build a one-mile roadway with 20 data observation locations as s_0 through s_{19} uniformly distributed. Assuming that an average vehicle length is 20 feet and the minimum gap between vehicles is 6 feet, the maximum vehicle density is thus around 203 vpm (vehicles per mile). We employ 2,000 particles (about 10 times of the vehicles) for simulating the traffic. The traffic flow rate gives the boundary condition at the starting end of the roadway. From the ground-truth data, we found that the traffic flow rate ranges from 500 vph (vehicles per hour) to around 2000 vph. Therefore, the corresponding rate of generating particles is around 1.4 to 5.6 particles per second in our simulation. We increase the traffic flow rate, and measure the density and the velocity after the traffic reaches a equilibrium state. The traffic and simulation parameters are reported in Tab. I. Here, the Greenfield

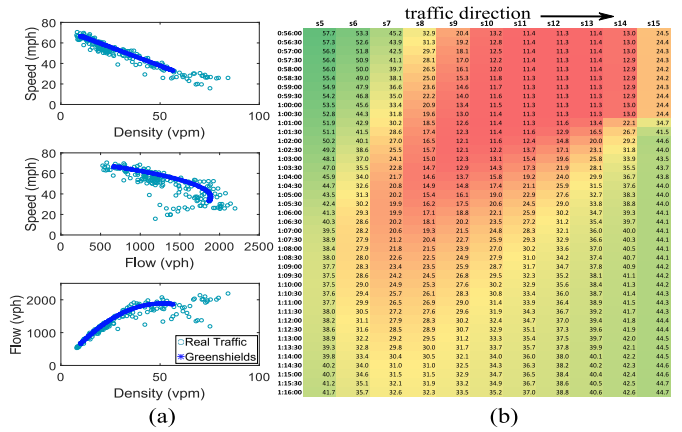


Fig. 7. The simulation results obtained from our downgraded model (i.e. the classic Greenshields model) well match the real-world observation.

model is used by setting $\gamma = 2.0$ (i.e. see Section III-D). The particle mass is a virtual quantity related to the traffic volume. We ignore the units of this quantity and other virtual-force related coefficients as well. We found the time step 0.025s is suitable for our simulation, considering the stability, efficiency and accuracy of the simulation. The performance depends on the simulation scale, e.g. it takes about 15 ms for advancing a step for the SPH simulation with 2,000 particles (with the single core implementation).

The simulation result of the fundamental diagram is reported in Fig. 7 (a). We also compare the congestion formation, transmission, and dissipation processes in Fig. 7 (b). The data at observation locations s_5 to s_{15} are presented. It can be seen that the simulated traffic appears less noisy and smoother than the real-world data, nevertheless they match each other well.

We further create an “artificial” crash event after the traffic reaches its equilibrium state and simulate how is the traffic congestion formed up and how does the shockwave transmit. The traffic velocity at the accident area is constrained to be zero to mimic the real traffic operations and to form up and the bottleneck. The congestion spreads out and the shockwave is transmitted backward from the high-density area to the low one. Eventually, after the crash is fully cleared up and the capacity is restored, the density distribution becomes uniform as the same as the initial state. The results are shown in Fig. 8.

B. CAV-Enabled Traffic Simulation

CAV-enabled traffic simulation is conducted using the original two-dimensional model with the standard full-kernel setting for the SPH simulator. The new fundamental diagram is shown in Fig. 9 (a), where we note that the speed is in fact the magnitude of the velocity vector obtained from the simulation. We can see that the CAV traffic flow is characterized by a quite different fundamental diagram compared to the traditional traffic flow model (Fig. 7 (a)). Rather than a straight line (one-to-one matching) characterized by the Greenshields model, the CAV speed-density relationship shows its over-dispersed distribution with all many-to-many matching patterns. One

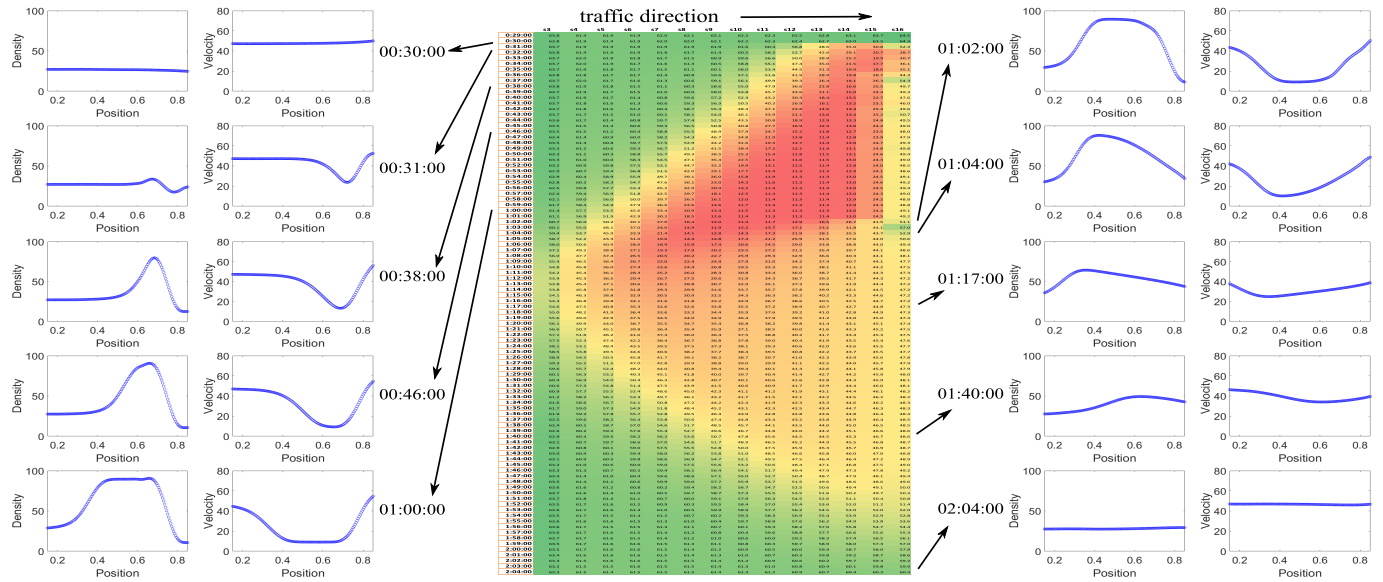


Fig. 8. The simulation results using our downgraded 1D model under an artificial congestion scenario are presented. We constrain the traffic velocity at the accident area to be zero. The resulting traffic congestion is visualized. The accident is cleared after 30 minutes and the traffic capacity is restored eventually.

single speed may correspond to multiple possible density states due to the two-way communication and collaborative linkages among CAVs. Similar results are observed in the flow-speed and flow-density relationships. For example, rather than a parabolic curve, the relationship between the flow and density tends to spread out as an area-wide distribution. Additionally, we can see that the traffic capacity is significantly improved in the CAV-enabled traffic as expected.

Fig. 9 (b) reports a distinctive congestion formation and dissipation pattern for the CAV-enabled traffic. Congestion can quickly spread out and transmit backward due to the timely communication among vehicles at such stronger magnitudes. These unique traffic equilibrium features and dynamic characteristics are different from these of traditional traffic flow. Further research efforts are needed to fully investigate their theoretical formulation based on the developed simulation models.

In the following experiments, we examine and visualize the variation of the density and velocity distribution under three scenarios individually. In the first scenario, all the forces are turned off except the pressure force f_p . The traffic density distribution is directly specified by the user to be highly nonuniform. Eventually, the distribution spreads out smoothly as shown in Fig. 10 (a). Similarly in the second scenario, only the viscous force f_v is turned on. One particle is activated and has a constant prescribed velocity. All other particles are stationary initially. As expected, the activated particle finally drives all particles to a certain velocity level as shown in Fig. 10 (b). In the third scenario, the traffic flow in a four-lane roadway is initially in an equilibrium state. An artificial crash event is created and two lanes (Lane 2 and 3) are blocked (shown in Fig. 10 (d)). The velocity within the accident area is constrained. We can see that the congestion transmits along both the traffic direction and the normal direction. The congestion can be partially mitigated

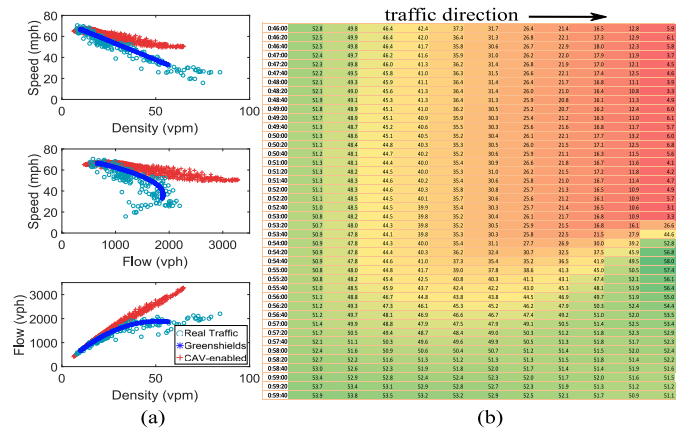


Fig. 9. The simulation results of testing the fundamental diagram and traffic dynamic characteristics in the CAV-enabled traffic using our model are presented.

through the available capacity from the adjacent lanes. This means that the proposed model not only can simulate the traffic flow along the traffic direction as existing traffic models do, but also can automatically handle the lane-changing behavior of the traffic flow (i.e. vehicles moving along the normal direction), because of its two-dimensional nature.

In order to better understand the CAV traffic flow characteristics, further experimental tests are conducted to quantify the dynamic performance of the developed model. The simulation results are shown in Fig. 11. We can see that although there is no accident in Lane 0, congestion formed and propagated. Note that we don't have an explicit lane-changing mechanism in the simulation, our model automatically handles the lane-changing requirement in this scenario. We also observe an interesting “speed up” area as highlighted in the figure. That is because the density in the upstream is high which increases the pressure force to push the downstream.

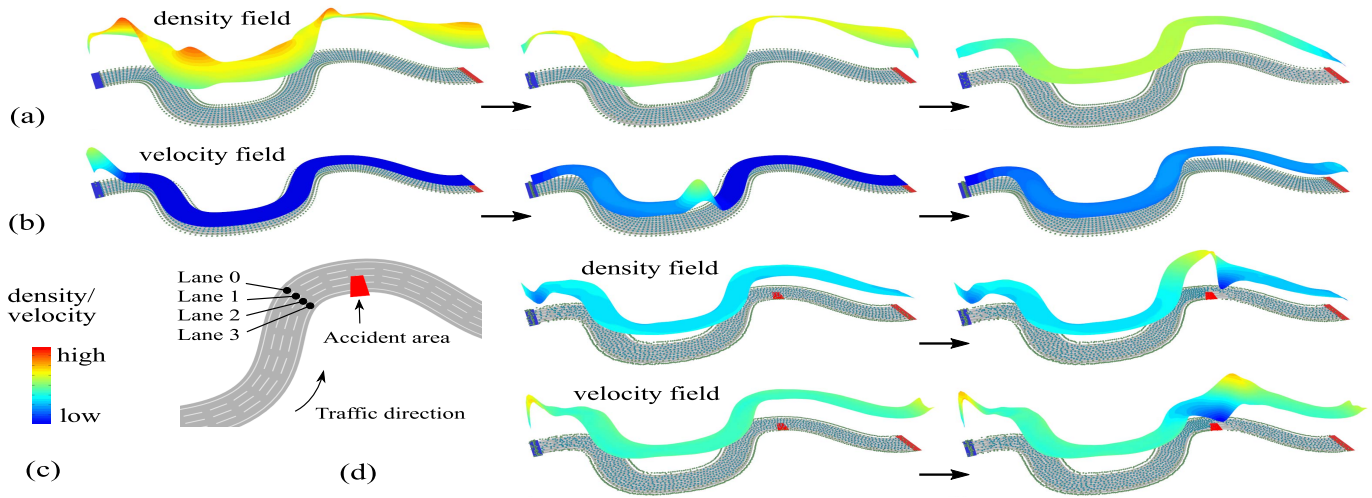


Fig. 10. The simulation results show how does the CAV-enabled traffic response to the imposed density change (a), velocity change (b), and under the traffic congestion (d). The color map (c) is associated with the density and velocity field, where red represents the highest value and blue the lowest value. Please refer to the accompanying video for details.

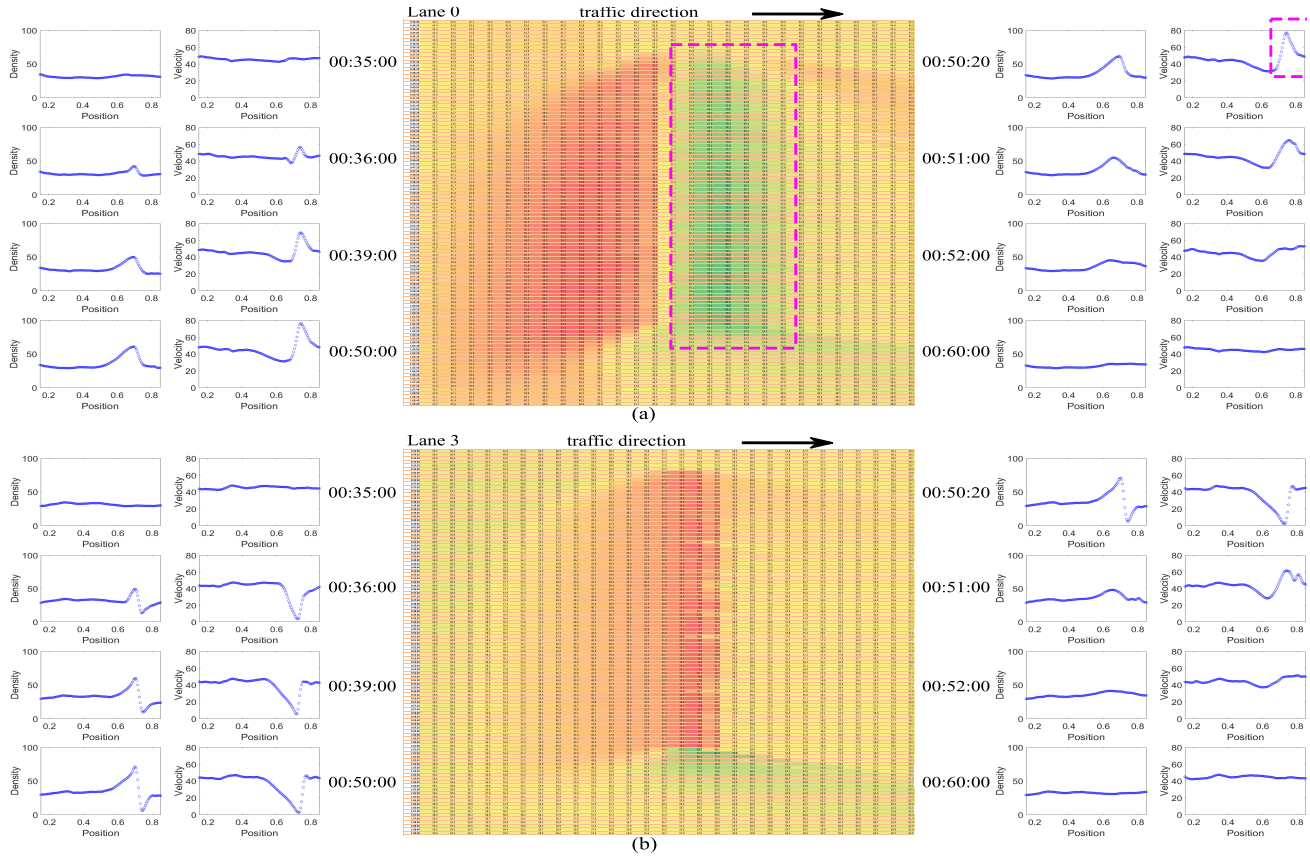


Fig. 11. The results of the congestion simulation in the CAV-enabled traffic. An artificial accident occurs at Lane 2 and 3 and the velocity within the accident area is constrained to zero. After 15 minutes, the accident is cleared. We can see that the congestion transmits not only horizontally (backward in Lane 2 and 3) but also vertically (to the adjacent Lane 0 and 1 where no accidents occurred though) due to the two-dimensional nature of our model. An interesting “speed-up” area in Lane 0 is also highlighted.

VI. CONCLUSIONS AND FUTURE WORK

In this study, a new force-driven continuum traffic flow model is proposed and SPH-based numerical solutions are provided. The proposed model amplifies neighborhood-wide vehicle coupling characterized in CAV-enabled traffic systems,

and individual vehicles spontaneously seek for local optimal configurations based on the real-time information shared/obtained from the surroundings. Inspired by the similarity between natural physical particle flow and CAV traffic flow, we formulate and simulate the mutually-coupled vehicle inter-

actions using internal virtual forces. Our experiment shows that the proposed model can be downgraded to incorporate the existing macroscopic traffic flow model and accurately describe the real-world traffic. Thus, there is a reason to believe this model works well in the context of CAV-enabled traffic systems too. Extensive experiments are conducted to illustrate the new fundamental diagram under the stationary equilibrium conditions and dynamic congestion formation/dissipation in the CAV-enabled traffic. Various operational scenarios are designed and tested to further demonstrate CAV traffic flow characteristics.

The developed CAV traffic flow model can advance our understanding of CAV-enabled traffic flow operations, facilitate near-future CAV-penetrated traffic management, quantify existing traffic facility capacity in the context of CAVs, and optimize mixed-traffic-to-infrastructure interactions. For example, based on the developed the model, various traffic operation management and control strategies can be tested theoretically and practically to verify their effectiveness before their implementations in CAV-enabled traffic flow. The latest share mobility modeling can be enhanced and smart decision making can be supported further in the interconnected and automated traffic environment. The theoretical insights extracted from the developed model can greatly facilitate CAV deployment in the entire traffic operation research domain.

In the future, we will test the proposed model with real CAV-enabled traffic data when it is sufficiently available. Currently, the virtual-force-based parameters in Table I are manually tuned. It would be an interesting topic that how we can formally relate those parameters to the real-world traffic flow. So far, the proposed virtual forces can only model the interaction of the CAVs in the same simulation domain or with the same traffic direction, and the information brought by the CAVs in the opposite direction is ignored. In order to handle the interaction between CAVs with opposite directions, we need to develop new types of virtual forces. Similarly, the proposed model is not sufficient for modeling the traffic with CAVs and human-driven vehicles mixed traffic behavior. This kind of interaction is basically asymmetric and might be modeled by some asymmetric virtual forces. We will put more efforts on the related research in the future.

In this work, we use the SPH-based method for the numerical simulation. It is also interesting to use grid-based simulation [72] instead of the particle-based one to simulate the proposed model. In this case, the convection (as appeared in Equation (5)) must be incorporated. We currently use full-kernel and half-kernel support in the CAV-enabled traffic and the conventional traffic respectively based on their different microscopic behavior. It is not clear yet how does the kernel function mathematically affect the fundamental diagram. Additionally, our current simulation is running only on CPU. We will further port our algorithm to GPU to fully leverage the parallelism of the SPH method.

ACKNOWLEDGEMENTS

The authors would like to thank T-ITS editors and reviewers for their constructive and detailed comments. Any opinions,

findings and conclusions or recommendations expressed in this material are those of the authors and do not necessarily reflect the views of funding agencies or others.

REFERENCES

- [1] P. J. Jin, C. M. Walton, G. Zhang, X. Jiang, and A. Singh, "Analyzing the impact of false-accident cyber attacks on traffic flow stability in connected vehicle environment," in *Proc. Int. Conf. Connected Vehicles Expo (ICCVE)*, Dec. 2013, pp. 616–621.
- [2] J. Hu, B. B. Park, and Y.-J. Lee, "Coordinated transit signal priority supporting transit progression under connected vehicle technology," *Transp. Res. C, Emerg. Technol.*, vol. 55, pp. 393–408, Jun. 2015.
- [3] T. Nobe, "Connected vehicle accelerates green driving," *SAE Int. J. Passenger Cars-Electron. Electr. Syst.*, vol. 3, no. 2, pp. 68–75, 2010.
- [4] A. Leon-Garcia, H.-A. Jacobsen, B. Adbulhai, M. Litoiu, and A. Tizghadam, *Connected Vehicles and Smart Transportation (CVST) Portal*. [Online]. Available: <https://www.utoronto.ca/news/challenge-u-engineering-team-oneeight-selected-develop-self-driving-electric-cars>
- [5] A. Leon-Garcia, "Smart Infrastructure and Applications for Connected Vehicles." Course Lecture, University of Toronto. Accessed: Feb. 4, 2018. [Online]. Available: <http://www.ece.ubc.ca/~vleung/CVWS2012/Toronto/Presentations/ALeon-Garcia.pdf>
- [6] A. Koulakezian and A. Leon-Garcia, "CVI: Connected vehicle infrastructure for ITS," in *Proc. IEEE 22nd Int. Symp. Pers. Indoor Mobile Radio Commun. (PIMRC)*, Sep. 2011, pp. 750–755.
- [7] A. Tizghadam and A. Leon-Garcia, "Robust network planning in nonuniform traffic scenarios," *Comput. Commun.*, vol. 34, no. 12, pp. 1436–1449, Aug. 2011.
- [8] D. Ticoll, "Driving changes: Automated vehicles in Toronto," Munk School Global Affairs, Univ. Toronto, Toronto, ON, Canada, Discussion Paper. Accessed: Feb. 4, 2018. [Online]. Available: <https://munkschool.utoronto.ca/ipf/files/2016/03/Driving-Changes-Ticoll-2015.pdf>
- [9] *University of Toronto is One of Eight Universities From Across North America Chosen to Compete in the Autodrive Challenge, Sponsored by GM and SAE International*. [Online]. Available: <https://www.utoronto.ca/news/challenge-u-engineering-team-one-eight-selected-develop-self-driving-electric-cars>
- [10] M. J. Lighthill and G. B. Whitham, "On kinematic waves. II. A theory of traffic flow on long crowded roads," *Proc. Roy. Soc. London, Ser. A, Math. Phys. Sci.*, vol. 229, no. 1178, pp. 317–345, 1955.
- [11] P. I. Richards, "Shock waves on the highway," *Oper. Res.*, vol. 4, no. 1, pp. 42–51, 1956.
- [12] P. Ross, "Traffic dynamics," *Transp. Res. B, Methodol.*, vol. 22, no. 6, pp. 421–435, 1988.
- [13] M. Papageorgiou, J.-M. Blosseville, and H. Hadj-Salem, "Macroscopic modelling of traffic flow on the Boulevard Périphérique in Paris," *Transp. Res. B, Methodol.*, vol. 23, no. 1, pp. 29–47, 1989.
- [14] P. G. Michalopoulos, D. E. Beskos, and J.-K. Lin, "Analysis of interrupted traffic flow by finite difference methods," *Transp. Res. B, Methodol.*, vol. 18, nos. 4–5, pp. 409–421, 1984.
- [15] H. M. Zhang, "A non-equilibrium traffic model devoid of gas-like behavior," *Transp. Res. B, Methodol.*, vol. 36, no. 3, pp. 275–290, 2002.
- [16] J. Lee, B. Park, K. Malakorn, and J. So, "Sustainability assessments of cooperative vehicle intersection control at an urban corridor," *Transp. Res. C, Emerg. Technol.*, vol. 32, pp. 193–206, Jul. 2013.
- [17] B. Andreianov, C. Donadello, and M. D. Rosini, "A second-order model for vehicular traffics with local point constraints on the flow," *Math. Models Methods Appl. Sci.*, vol. 26, no. 4, pp. 751–802, 2016.
- [18] D. Wang, X. Ma, D. Ma, and S. Jin, "A novel speed-density relationship model based on the energy conservation concept," *IEEE Trans. Intell. Transp. Syst.*, vol. 18, no. 5, pp. 1179–1189, May 2017.
- [19] K. Leonard, "Keeping the promise of connected vehicle technology: Toward an era of unprecedented roadway safety and efficiency," *TR News*, vol. 285, pp. 3–9, 2013.
- [20] T. Litman, *Autonomous Vehicle Implementation Predictions*, vol. 28. Victoria, BC, Canada: Victoria Transport Policy Inst., 2014.
- [21] D. Ni, J. Li, S. Andrews, and H. Wang, "A methodology to estimate capacity impact due to connected vehicle technology," *Int. J. Veh. Technol.*, vol. 2012, 2011, Art. no. 502432.
- [22] C. Wu, S. Ohzahata, Y. Ji, and T. Kato, "How to utilize interflow network coding in VANETs: A backbone-based approach," *IEEE Trans. Intell. Transp. Syst.*, vol. 17, no. 8, pp. 2223–2237, Aug. 2016.

- [23] J. I. Ge and G. Orosz, "Dynamics of connected vehicle systems with delayed acceleration feedback," *Transp. Res. C, Emerg. Technol.*, vol. 46, pp. 46–64, Sep. 2014.
- [24] Y. Feng, K. L. Head, S. Khoshmagham, and M. Zamanipour, "A real-time adaptive signal control in a connected vehicle environment," *Transp. Res. C, Emerg. Technol.*, vol. 55, pp. 460–473, Jun. 2015.
- [25] J. Du and M. J. Barth, "Next-generation automated vehicle location systems: Positioning at the lane level," *IEEE Trans. Intell. Transp. Syst.*, vol. 9, no. 1, pp. 48–57, Mar. 2008.
- [26] H. Park, "Development of ramp metering algorithms using individual vehicular data and control under vehicle infrastructure integration," Ph.D. dissertation. Univ. Virginia, Charlottesville, VA, USA, 2008.
- [27] M. A. Togou, A. Hafid, and L. Khoukhi, "SCRIP: Stable CDS-based routing protocol for urban vehicular ad hoc networks," *IEEE Trans. Intell. Transp. Syst.*, vol. 17, no. 5, pp. 1298–1307, May 2016.
- [28] M. A. S. Kamal, S. Taguchi, and T. Yoshimura, "Efficient driving on multilane roads under a connected vehicle environment," *IEEE Trans. Intell. Transp. Syst.*, vol. 17, no. 9, pp. 2541–2551, Sep. 2016.
- [29] J. Lee and B. Park, "Development and evaluation of a cooperative vehicle intersection control algorithm under the connected vehicles environment," *IEEE Trans. Intell. Transp. Syst.*, vol. 13, no. 3, pp. 81–90, Mar. 2012.
- [30] M. A. S. Kamal, J.-I. Imura, T. Hayakawa, A. Ohata, and K. Aihara, "A vehicle-intersection coordination scheme for smooth flows of traffic without using traffic lights," *IEEE Trans. Intell. Transp. Syst.*, vol. 16, no. 3, pp. 1136–1147, Jun. 2015.
- [31] L. Zha, Y. Zhang, P. Songchitruksa, and D. R. Middleton, "An integrated dilemma zone protection system using connected vehicle technology," *IEEE Trans. Intell. Transp. Syst.*, vol. 17, no. 6, pp. 1714–1723, Jun. 2016.
- [32] K. Tiaprasert, Y. Zhang, X. B. Wang, and X. Zeng, "Queue length estimation using connected vehicle technology for adaptive signal control," *IEEE Trans. Intell. Transp. Syst.*, vol. 16, no. 4, pp. 2129–2140, Aug. 2015.
- [33] P. Lytrivis, G. Thomaidis, M. Tsogas, and A. Amditis, "An advanced cooperative path prediction algorithm for safety applications in vehicular networks," *IEEE Trans. Intell. Transp. Syst.*, vol. 12, no. 3, pp. 669–679, Sep. 2011.
- [34] A. Y. S. Lam, Y.-W. Leung, and X. Chu, "Autonomous-vehicle public transportation system: Scheduling and admission control," *IEEE Trans. Intell. Transp. Syst.*, vol. 17, no. 5, pp. 1210–1226, May 2016.
- [35] L. Du and H. Dao, "Information dissemination delay in vehicle-to-vehicle communication networks in a traffic stream," *IEEE Trans. Intell. Transp. Syst.*, vol. 16, no. 1, pp. 66–80, Feb. 2015.
- [36] O. A. Osman and S. Ishak, "A network level connectivity robustness measure for connected vehicle environments," *Transp. Res. C, Emerg. Technol.*, vol. 53, pp. 48–58, Apr. 2015.
- [37] J. Monteil, R. Billot, J. Sau, and N.-E. El Faouzi, "Linear and weakly nonlinear stability analyses of cooperative car-following models," *IEEE Trans. Intell. Transp. Syst.*, vol. 15, no. 5, pp. 2001–2013, Oct. 2014.
- [38] R. Cheng, H. Ge, and J. Wang, "An extended continuum model accounting for the driver's timid and aggressive attributions," *Phys. Lett. A*, vol. 381, no. 15, pp. 1302–1312, 2017.
- [39] L. Zheng, Z. He, and T. He, "A flexible traffic stream model and its three representations of traffic flow," *Transp. Res. C, Emerg. Technol.*, vol. 75, pp. 136–167, Feb. 2017.
- [40] D. C. Gazis, R. Herman, and R. B. Potts, "Car-following theory of steady-state traffic flow," *Oper. Res.*, vol. 7, no. 4, pp. 499–505, 1959.
- [41] G. Asaithambi, V. Kanagaraj, and T. Toledo, "Driving behaviors: Models and challenges for non-lane based mixed traffic," *Transp. Develop. Econ.*, vol. 2, Oct. 2016, Art. no. 19.
- [42] L. Guo, X. Zhao, S. Yu, X. Li, and Z. Shi, "An improved car-following model with multiple preceding cars' velocity fluctuation feedback," *Phys. A, Statist. Mech. Appl.*, vol. 471, pp. 436–444, Apr. 2017.
- [43] Z. Li, X. Xu, S. Xu, and Y. Qian, "A heterogeneous traffic flow model consisting of two types of vehicles with different sensitivities," *Commun. Nonlinear Sci. Numer. Simul.*, vol. 42, pp. 132–145, Jan. 2017.
- [44] M. Garavello and B. Piccoli, "Boundary coupling of microscopic and first order macroscopic traffic models," *Nonlinear Differential Equations Appl. NoDEA*, vol. 24, no. 4, p. 43, 2017.
- [45] H. Holden and N. H. Risebro. (2017). "Follow-the-Leader models can be viewed as a numerical approximation to the Lighthill-Whitham-Richards model for traffic flow." [Online]. Available: <https://arxiv.org/abs/1702.01718>
- [46] S. Chiappone, O. Giuffrè, A. Granà, R. Mauro, and A. Sferlazza, "Traffic simulation models calibration using speed–density relationship: An automated procedure based on genetic algorithm," *Expert Syst. Appl.*, vol. 44, pp. 147–155, Feb. 2016.
- [47] F. Zhu and S. V. Ukkusuri, "An optimal estimation approach for the calibration of the car-following behavior of connected vehicles in a mixed traffic environment," *IEEE Trans. Intell. Transp. Syst.*, vol. 18, no. 2, pp. 282–291, Feb. 2017.
- [48] R. X. Zhong, K. Y. Fu, A. Sumalee, D. Ngoduy, and W. H. K. Lam, "A cross-entropy method and probabilistic sensitivity analysis framework for calibrating microscopic traffic models," *Transp. Res. C, Emerg. Technol.*, vol. 63, pp. 147–169, Feb. 2016.
- [49] J. Zhao and S. Sun, "High-order Gaussian process dynamical models for traffic flow prediction," *IEEE Trans. Intell. Transp. Syst.*, vol. 17, no. 7, pp. 2014–2019, Jul. 2016.
- [50] G. Zhang, X. Ma, and Y. Wang, "Self-adaptive tolling strategy for enhanced high-occupancy toll lane operations," *IEEE Trans. Intell. Transp. Syst.*, vol. 15, no. 1, pp. 306–317, Feb. 2014.
- [51] X. Liu, G. Zhang, C. Kwan, Y. Wang, and B. Kemper, "Simulation-based, scenario-driven integrated corridor management strategy analysis," *Transp. Res. Rec., J. Transp. Res. Board*, vol. 2396, pp. 38–44, 2013.
- [52] G. Zhang and Y. Wang, "Optimizing coordinated ramp metering: A preemptive hierarchical control approach," *Comput.-Aided Civil Infrastruct. Eng.*, vol. 28, no. 1, pp. 22–37, 2013.
- [53] G. Zhang and Y. Wang, "Optimizing minimum and maximum green time settings for traffic actuated control at isolated intersections," *IEEE Trans. Intell. Transp. Syst.*, vol. 12, no. 1, pp. 164–173, Mar. 2011.
- [54] G. Zhang, S. Yan, and Y. Wang, "Simulation-based investigation on high-occupancy toll lane operations for Washington state route 167," *J. Transp. Eng.*, vol. 135, no. 10, pp. 677–686, 2009.
- [55] G. Zhang, Y. Wang, H. Wei, and P. Yi, "A feedback-based dynamic tolling algorithm for high-occupancy toll lane operations," *Transp. Res. Rec., J. Transp. Res. Board*, vol. 2065, pp. 54–63, 2008.
- [56] M. Rieser, K. Nagel, U. Beuck, M. Balmer, and J. Rümennapp, "Agent-oriented coupling of activity-based demand generation with multiagent traffic simulation," *Transp. Res. Rec., J. Transp. Res. Board*, vol. 2021, pp. 10–17, 2007.
- [57] S. Adhikari, "Damping modelling using generalized proportional damping," *J. Sound Vibrat.*, vol. 293, nos. 1–2, pp. 156–170, 2006.
- [58] R. Temam, *Navier-Stokes Equations*, vol. 2. Amsterdam, The Netherlands: North Holland, 1984.
- [59] M. Müller, D. Charypar, and M. Gross, "Particle-based fluid simulation for interactive applications," in *Proc. ACM SIGGRAPH/Eurograph. Symp. Comput. Animation*, 2003, pp. 154–159.
- [60] L. B. Lucy, "A numerical approach to the testing of the fission hypothesis," *Astron. J.*, vol. 82, pp. 1013–1024, Dec. 1977.
- [61] R. A. Gingold and J. J. Monaghan, "Smoothed particle hydrodynamics: Theory and application to non-spherical stars," *Monthly Notices Roy. Astron. Soc.*, vol. 181, no. 3, pp. 375–389, 1977.
- [62] J. J. Monaghan, "Smoothed particle hydrodynamics," *Annu. Rev. Astron. Astrophys.*, vol. 30, no. 1, pp. 543–574, 1992.
- [63] M. B. Liu and G. R. Liu, "Smoothed particle hydrodynamics (SPH): An overview and recent developments," *Arch. Comput. Methods Eng.*, vol. 17, no. 1, pp. 25–76, 2010.
- [64] J. Stam and E. Fiume, "Depicting fire and other gaseous phenomena using diffusion processes," in *Proc. 22nd Annu. Conf. Comput. Graph. Interact. Techn.*, 1995, pp. 129–136.
- [65] B. Solenthaler, P. Bucher, N. Chentanez, M. Müller, and M. Gross, "SPH based shallow water simulation," in *Proc. 8th Workshop Virtual Reality Interact. Phys. Simulations (VRIPHYS)*, Lyon, France, 2011, pp. 39–46.
- [66] H. Rakha and B. Crowther, "Comparison of greenshields, pipes, and van aerde car-following and traffic stream models," *Transp. Res. Rec., J. Transp. Res. Board*, vol. 1802, pp. 248–262, 2002.
- [67] R. P. Fedkiw, T. Aslam, B. Merriman, and S. Osher, "A non-oscillatory eulerian approach to interfaces in multimaterial flows (the ghost fluid method)," *J. Comput. Phys.*, vol. 152, no. 2, pp. 457–492, 1999.
- [68] R. P. Fedkiw, "Coupling an eulerian fluid calculation to a Lagrangian solid calculation with the ghost fluid method," *J. Comput. Phys.*, vol. 175, no. 1, pp. 200–224, 2002.
- [69] H. Schechter and R. Bridson, "Ghost SPH for animating water," *ACM Trans. Graph.*, vol. 31, no. 4, 2012, Art. no. 61.
- [70] S. J. Cummins and M. Rudman, "An SPH projection method," *J. Comput. Phys.*, vol. 152, no. 2, pp. 584–607, 1999.

- [71] B. Heidelberger, M. Teschner, R. Keiser, M. Müller, and M. Gross, "Consistent penetration depth estimation for deformable collision response," in *Proc. Vis., Modeling, Vis. (VMV)*, Stanford, CA, USA, 2004, pp. 339–346.
- [72] R. Bridson, *Fluid Simulation for Computer Graphics*. Boca Raton, FL, USA: CRC Press, 2015.



Yuming Zhang received the M.S. degree in electrical engineering from the Institute of Electrical Engineering, China Academy Science, in 2002. He is currently pursuing the Ph.D. degree with the Department of Electrical and Computer Engineering, University of New Mexico. He is currently a Research Assistant with the Department of Electrical and Computer Engineering, University of New Mexico. His research interests include physics-based animation/simulation, non-linear system analysis, scientific visualization, image processing, transportation data

analysis, and large-scale traffic flow simulation.



Guohui Zhang received the Ph.D. degree from the University of Washington, Seattle, WA, USA, in 2000. He is currently an Assistant Professor with the Department of Civil and Environmental Engineering, University of Hawaii at Manoa, Honolulu, HI, USA. His research interests include transportation system operations and analysis, transportation data management and analysis, large-scale traffic simulation, geographic information system-based infrastructure asset management, and traffic detection systems.



Rafael Fierro received the Ph.D. degree in electrical engineering from the University of Texas at Arlington in 1997. Prior to joining the Systems and Controls Group, Department of Electrical and Computer Engineering, University of New Mexico, in 2007, he held a post-doctoral appointment with the GRASP Lab, University of Pennsylvania and a Faculty Member with the Department of Electrical and Computer Engineering, Oklahoma State University. His research interests include hybrid and embedded systems, heterogeneous multivehicle coordination, cooperative and distributed control of multi-agent systems, mobile sensor networks, and robotics.



Yin Yang received the Ph.D. degree in computer science from the University of Texas at Dallas in 2013. He is an Assistant Professor with the Department of Electrical Computer Engineering, University of New Mexico, Albuquerque, NM, USA. His research interests include physics-based animation/simulation and related applications, scientific visualization, and medical imaging analysis.